E-Journal of Advanced Maintenance Vol. 13 No. 1 (2021) 1-11
Japan Society of Maintenology

Tempering Effect Prediction of Temper Bead Repair Technology for BMI Penetration Nozzles

Lina YU[1,*], Kazuyoshi SAIDA[1], Kazutoshi NISHIMOTO[1] and Naoki CHIGUSA[2]

[1] *Osaka University, 2-1 Yamadaoka, Suita, Osaka 565-0871, Japan*
[2] *The Kansai Electric Power Co., Inc., 8 Yokota, 13 Goichi, Mihama-cho, Mikata-gun, Fukui 919-1141, Japan*

ABSTRACT

The aged reactor vessel bottom mounted instrument (BMI) penetration nozzles of nuclear power plant needs to be repaired or maintained. Temper bead welding is one effective repair welding methods instead of post weld heat treatment. For temper bead welding, hardness and toughness are the key criteria to evaluate the tempering effect. A neural network-based method for hardness and toughness prediction in heat affected zone of low-alloy steel has been constructed to evaluate the tempering effect in temper bead welding by the authors. For the BMI penetration nozzle with different mounting angles (0°, 15°, 30°and 45°), the hardness and toughness distribution in heat affected zone of temper bead welding in the cross sections of BMI penetration nozzle was predicted based on the thermal cycles numerically obtained by Finite Element Method (FEM). Through this method, the tempering effect of the temper bead repair technology can be predicted before the actual repair welding, thus the appropriate welding conditions would be able to optimize before the actual repair welding, which was very useful for the repair welding for BMI penetration nozzles of nuclear power plant.

KEYWORDS

BMI, Hardness, Toughness, Temper bead welding, low-alloy steel, FEM

ARTICLE INFORMATION

Article history:
Received October 2020
Accepted May 2021

1. Introduction

A bottom mounted instrument (BMI) penetration nozzle is a tube welded into the reactor vessel bottom. Its role is to allow the introduction of nuclear instrumentation into the core of the reactor. A leak in the BMI tube or J-weld constitutes a break of the primary coolant system. BMI nozzles in bottom head of the nuclear reactor pressure vessel are one of the pressure boundaries in reactor coolant system for inspection of weld cracking, also, the BMI nozzle welds form part of the primary pressure boundary and the weld filler material is of alloy 600 which is known to be susceptible to primary water stress corrosion cracking (PWSCC) which is one of important metallurgical problems facing the nuclear industry [1,2]. Low alloy steel ASTM A533B possessing superior low-temperature toughness and weldability is typically used as the material for pressurized water reactor vessels in nuclear power plants. The aged nuclear power plants are needed to be repaired or maintained to assure the safety and extend their lives. After repair welding, post weld heat treatment (PWHT) is normally required to eliminate the residual stress and decrease the hardness. However, PWHT is sometimes difficult to perform in operation in the case of repairing for large-scale structures. In practice, the temper bead welding technique is an effective repair welding method instead of PWHT [3-5].

Temper bead welding is a kind of multi-pass welding, in which the tempering effect is caused by heat-arising from the subsequent multi-layer weld thermal cycles. For temper bead welding, hardness and toughness are the key criteria to evaluate the tempering effect. The authors have previously reported the hardness and toughness prediction systems of the temper bead welding technique using neural network based on the experimentally obtained hardness and toughness database [6-7]. And the effectivity for the plain surface has been proved.

However, for the repair welding of BMI penetration nozzle, the welding surface is not the plain surface and sometime there are different angles between the BMI and the vessel bottom in practical operation. Therefore, in the present study, the hardness and toughness prediction in heat affected zone

* Corresponding author, E-mail: yulina@mapse.osaka-u.ac.jp

(HAZ) of temper bead welding of BMI penetration nozzle with different mounting angles (0°, 15°, 30°and 45°) has been investigated based on the thermal cycles numerically obtained by Finite Element Method. Through this method, the tempering effect of the temper bead repair technology can be predicted before the actual repair welding, thus the appropriate welding conditions would be able to optimize before repair welding, which was very useful for the repair welding for BMI penetration nozzles of nuclear power plant.

2. FEM models of BMI penetration

In order to simulate the actual repair welding of BMI penetration nozzle with the mounting angle of 0°, FEM model of multi-pass circle welded samples were produced by Patran, as shown in Fig. 1. As illustrated in Fig. 1 (b), the union between the bottom of the vessel (stainless steel SUS304 cladding layer) and the BMI Nozzle (Alloy 600) was formed by a buttering and a J-groove weld with Alloy 690, and the other part is low-alloy steel A533B. The dimensions of the groove shape and the thickness of SUS304 cladding were shown in Fig. 1(b).

The welding conditions of the multi-pass welding were shown in Table 1. The welding speed was set as 2 mm/s for all pass welding. The heat input of the first layer (1^{st} pass ~ 11^{th} pass) welding was set as 700 J/mm, while the heat input from the second layer (12^{th} pass ~ 50^{th} pass) welding was arranged as 1050 J/mm, which is higher than that of the first layer welding. And the built-up sequence in the cross section was illustrated in Fig. 2. For the heat input of 700 J/mm, the average bead width and beat height was set as 4 mm and 2.6 mm respectively. While the average bead width and beat height were changed to 4 mm and 4 mm for the heat input of 1050 J/mm. In order to better simulate the thermal history of weld metal well, the mesh size was set as about 1.3mm, and the mesh size in HAZ near to weld metal is little coarser than that of weld metal. On the other hand, the mesh in the base metal far from the weld metal was much rougher to reduce the simulation time.

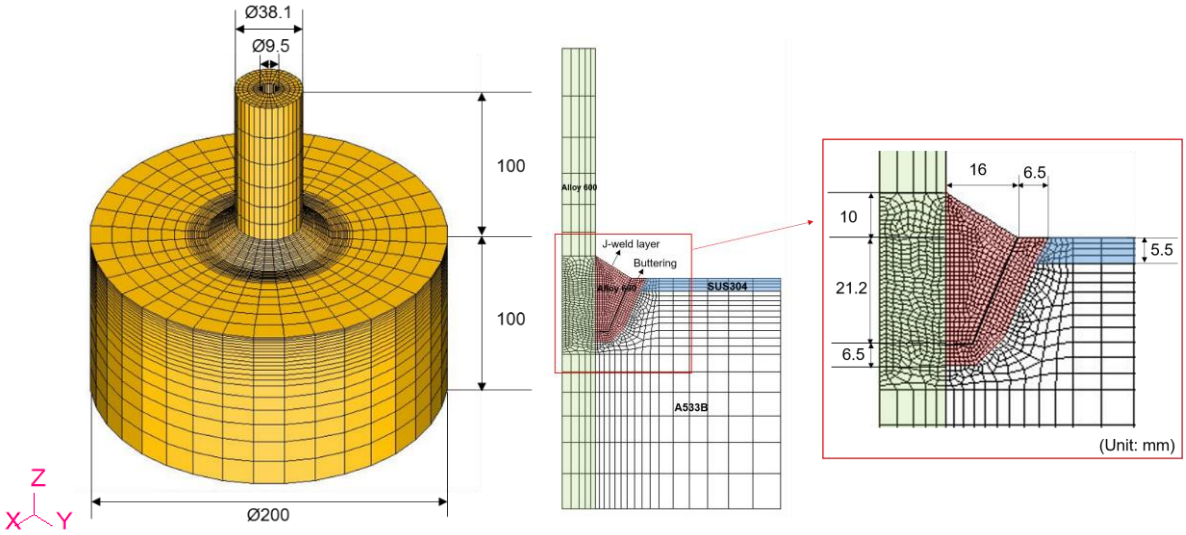

(a) 3D model (b) cross section of the model

Fig. 1 Finite element model of BMI nozzle with the angle of 0°

Table 1 Welding conditions of multi-pass welding

1^{st} pass ~ 11^{th} pass	Heat Input, Q (J/mm)	700
	Welding Speed, v (mm/s)	2.0
12^{th} pass ~ 50^{th} pass	Heat Input, Q (J/mm)	1050
	Welding Speed, v (mm/s)	2.0

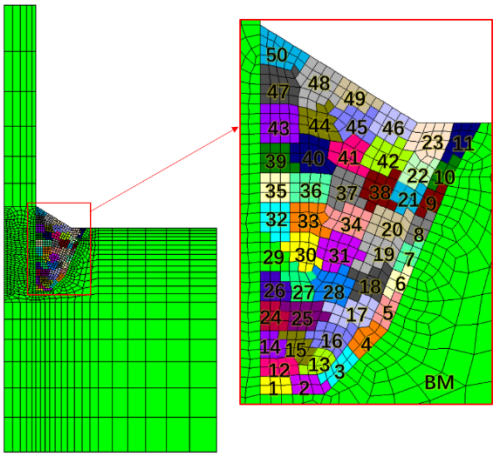

Fig. 2 Built-up sequence

Because the actual BMI penetration nozzle always have some angle with the reactor vessel bottom, the FEM models of BMI penetration nozzles with 15°, 30° and 45° mounting angles were also constructed as illustrated in Fig. 3. Every overlay welding was performed by 2 passes of semi-circle, with the welding directions shown in Fig. 4. And the hardness and toughness of the start section (θ = 0°) and the end section (θ = 180°) were mainly investigated in this study.

The thermal cycles in multi-pass temper bead welding were calculated using FEM software developed for welding simulation [8]. The temperature dependencies of physical properties of A533B, Alloy 600, Alloy 690 and SUS304 were illustrated in Tables 2-3 and Figs. 5-6, respectively.

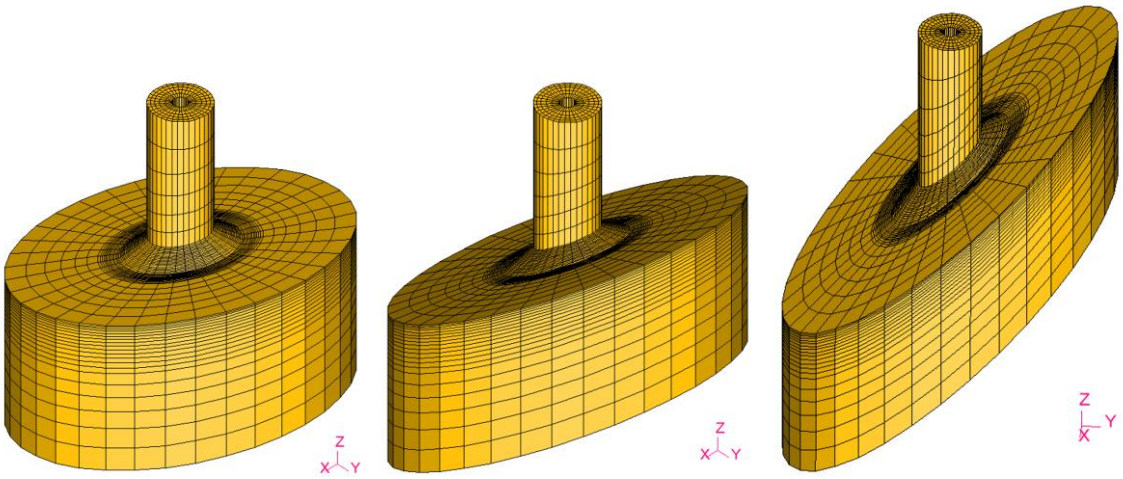

(a) 15° (b) 30° (c) 45°

Fig. 3 Finite element model of BMI nozzle with different mounting angles

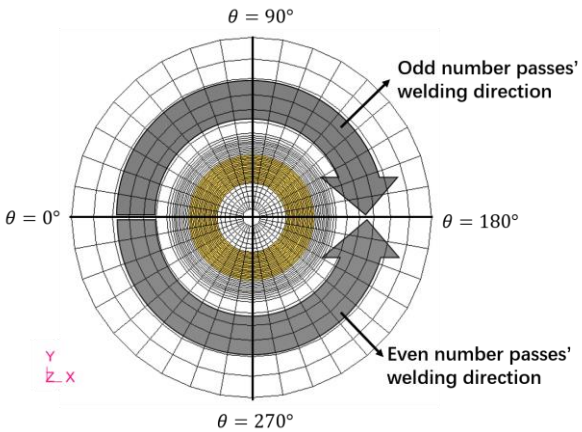

Fig. 4 Welding direction from the top view

Table 2 Temperature dependencies of physical properties of A533B steel

Temperature (℃)	Specific heat (J/kg℃)	Thermal conductivity (W/mm℃)	Yield Strength (MPa)	Young's modulus (GPa)	Possion's ratio (—)	Thermal expansion (1/℃)
20	445	0.039	478	210	0.3	12.0e-6
200	517	0.0389	455	202	0.3	12.7e-6
400	592	0.036	405	188	0.3	13.9e-6
600	723	0.0317	238	160	0.3	13.8e-6
800	812	0.0378	75	115	0.3	12.6e-6
1000	658	0.0309	17	93	0.3	12.6e-6
1300	721	0.0365	5	10	0.3	14.5e-6

Table 3 Temperature dependencies of physical properties of Alloy 600

Temperature (℃)	Specific heat (J/kg℃)	Thermal conductivity (W/mm℃)	Young's modulus (GPa)	Possion's ratio (—)
20	444	0.0149	214	0.324
100	465	0.0159	210	0.319
200	486	0.0173	205	0.314
300	502	0.0190	199	0.306
400	519	0.0205	193	0.301
500	536	0.0221	187	0.300
600	578	0.0239	180	0.301
700	595	0.0257	172	0.305
800	611	0.0275	164	0.320
900	628	0.0285	154	0.330

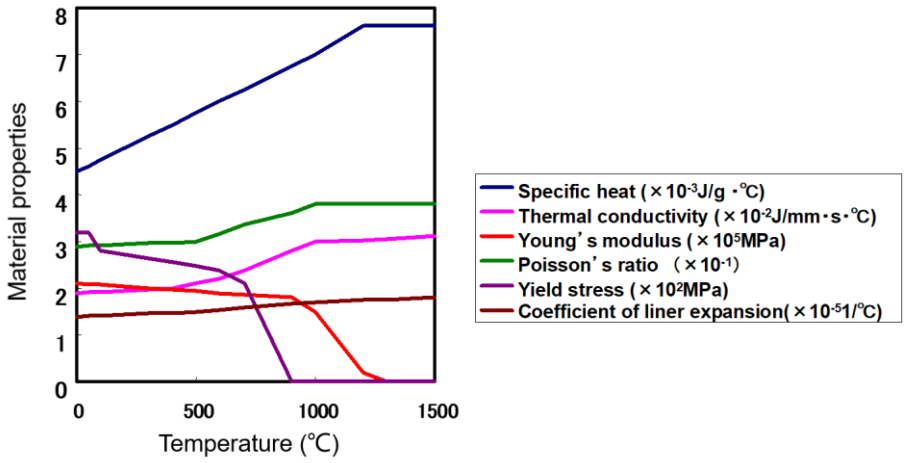

Fig. 5 Temperature dependencies of physical properties of Alloy 690.

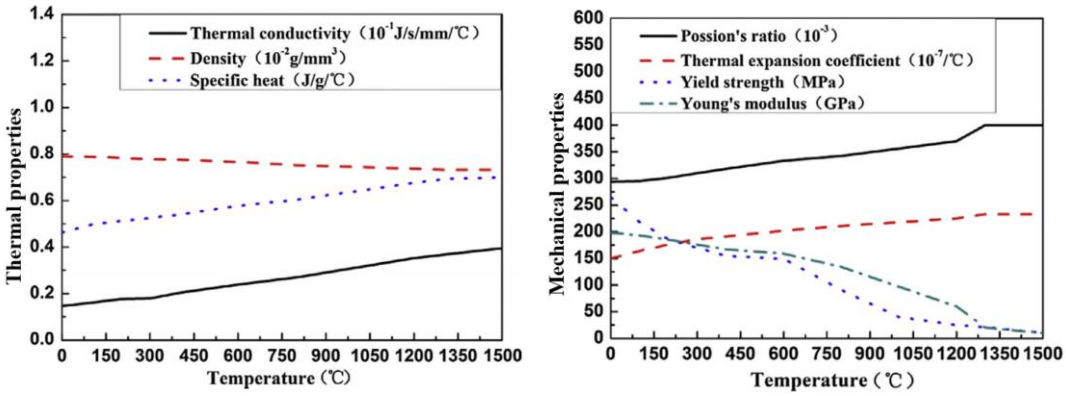

Fig. 6 Temperature dependencies of physical properties of SUS304.

3. Neural Network-based hardness and toughness prediction systems

Because the mechanical properties such and hardness and toughness in HAZ subjected to various kinds of thermal cycles is determined by the parameters: T_{pi}, CR_i and TCTP [6,7], the prediction systems of hardness/toughness were constructed with using a Neural Network (NN). T_{pi} is the peak temperature of the i^{th} pass thermal cycle, CR_i means the cooling rate from 800℃ to 500℃ of the i^{th} pass thermal cycle (When the T_p of the thermal cycle is lower than 800℃, the cooling rate at 400℃ is taken as CR). And the tempering effect of all the temper thermal cycles can be considered to be expressed as a factor, TCTP (Thermal cycle tempering parameter), proposed by the authors, by extending the Larson-Miller parameter (LMP) to non-isothermal heat treatment [6].

The NN [9,10] method is a powerful tool which can process such complex data as involved in the present research. NN is a mathematical model or computational model that simulates the structure and/or functional aspects of biological neural networks. In most cases, a NN is an adaptive system that changes its structure based on external or internal information that flows through the network during the learning phase. Modern neural networks have become useful modeling tools for non-linear statistical data. They are usually used to model complex relationships between inputs and outputs or to find patterns in data.

The radial basis function (RBF) [11] is a powerful technique for interpolation of multidimensional space in a NN. Fig. 7 illustrates the RBF-NN model. RBF networks typically have three layers: an input layer, a hidden layer with a non-linear RBF activation function and a linear output layer. The hidden layer can be described by a Gaussian basis function:

$$h(x) = \exp\{-(x-c)^2/r^2\} \quad (1)$$

where x is the input data, c is the center vector, and r is the euclidean distance. In the basic form all inputs are connected to each hidden neuron.

The output $O(x_i)$ of the network is thus

$$O(x_i) = \sum_{j=1}^{n} w_j\, h_j(x_i) = \sum_{j=1}^{n} w_j \exp\{-(x_i - c_j)^2/r^2\} \quad (2)$$

where *n* is the number of neurons in the hidden layer, c_j is the center vector for neuron j, and w_j are the weights of the linear output neuron. The weights w_j, c_j, and r are determined in a manner that optimizes the fit between $O(x_i)$ and the data. In the present study, the thermal cycle parameters (T_{pi}, CR_i and TCTP) are the input data, and the hardness/toughness is the output data.

Therefore, based on the experimentally obtained hardness/toughness database, the neural network-based hardness and toughness prediction systems have been constructed by the authors [6,7].

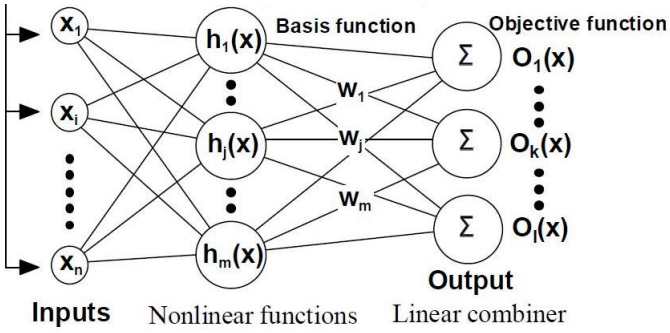

Fig. 7 Radial basis function neural network model

4. Temperature analysis of multi-pass welding in BMI penetration nozzle by FEM simulation

The temperature distributions produced by multi-pass thermal cycles in welds during buttering and J-welding in BMI penetration nozzle were calculated using three-dimensional finite element analysis code, developed specifically for welding simulation. Figs. 8-11 presented the calculated peak temperature distribution of BMI penetration nozzles with the mounting angles varied as 0°, 15°, 30°and 45°, respectively. Peak temperatures were presented in different color scale according to the different temperature levels. And the peak temperature was shown from the 3D view and the top view. And from the top view, there was no marked difference in the peak temperature distribution after multi-pass welding when the mounting angles varied from 0° to 45°.

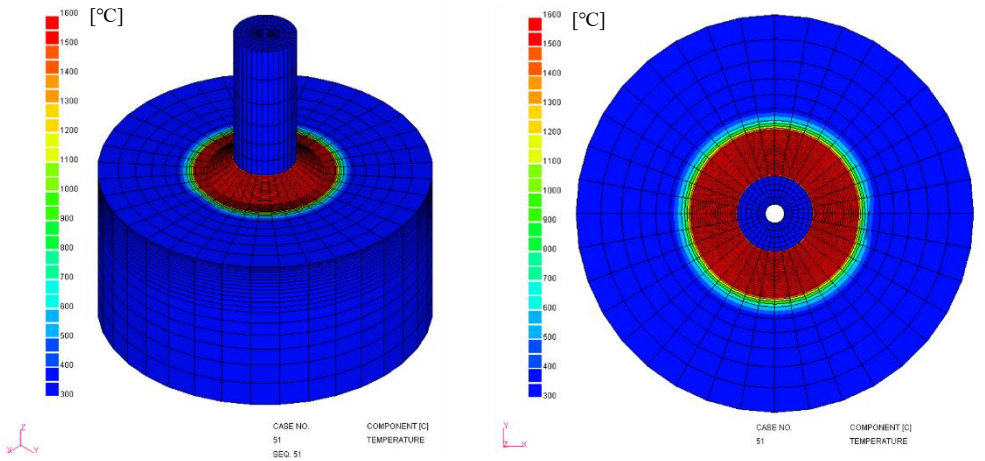

(a) 3D view (b) Top view

Fig. 8 Simulated peak temperature distribution in BMI nozzle after multi-pass welding with the mounting angle of 0°

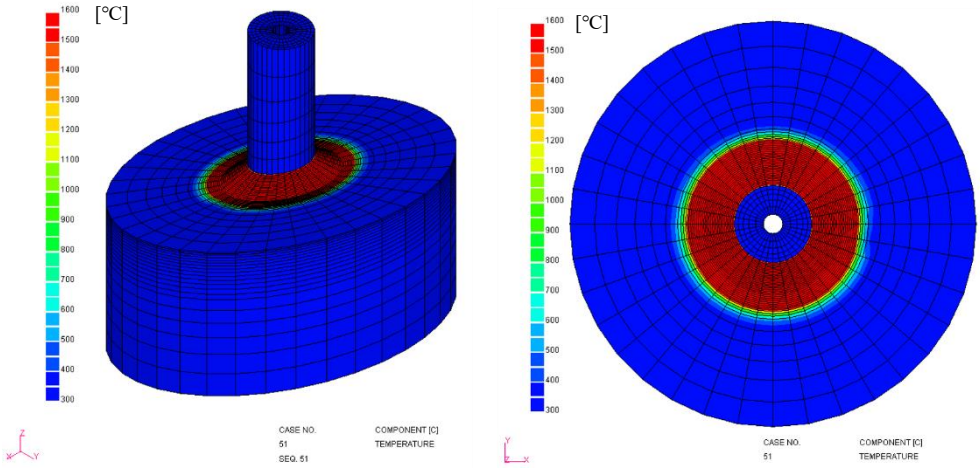

(a) 3D view (b) Top view

Fig. 9 Simulated peak temperature distribution in BMI nozzle after 50 pass welding with the mounting angle of 15°

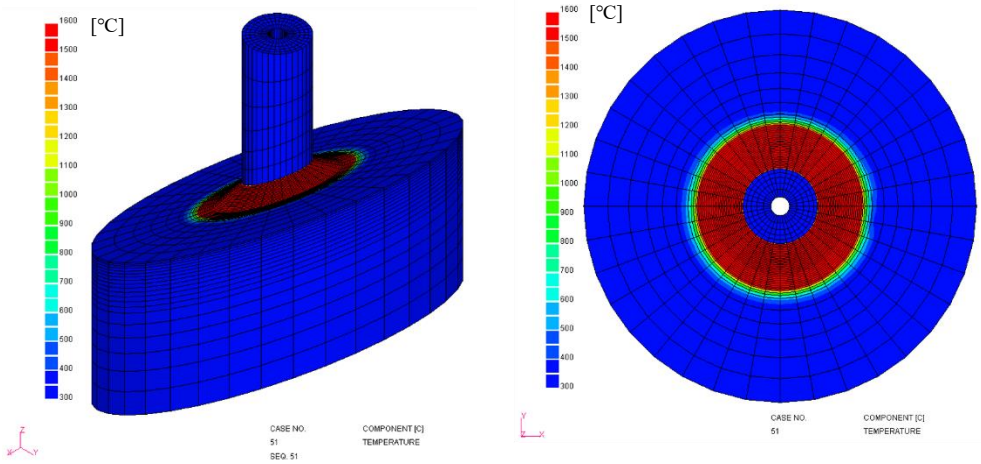

(a) 3D view (b) Top view

Fig. 10 Simulated peak temperature distribution in BMI nozzle after 50 pass welding with the mounting angle of 30°

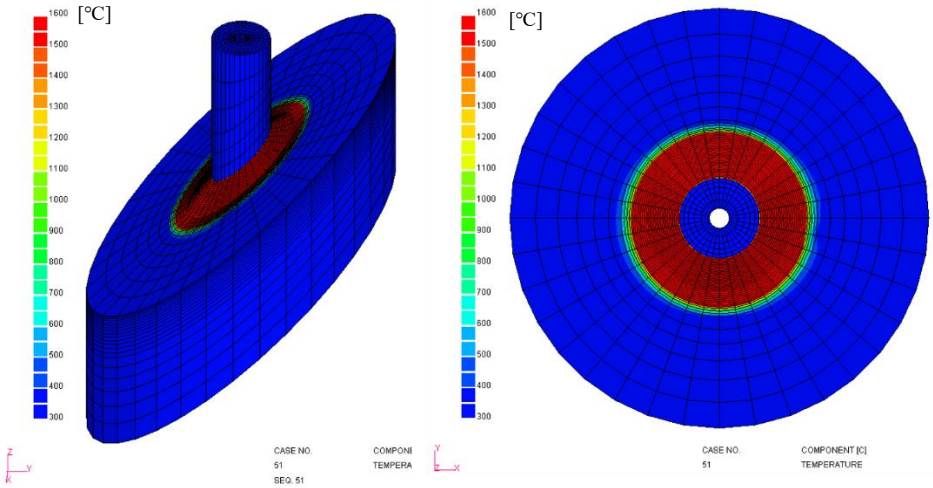

(a) 3D view (b) Top view

Fig. 11 Simulated peak temperature distribution in BMI nozzle after 50 pass welding with the mounting angle of 45°

5. Predicted hardness distribution in the cross section of BMI penetration nozzle with different mounting angles

Based on the calculated thermal history at all grid nodes of the mesh, the hardness at the grid nodes of the cross section of BMI penetration nozzle was calculated, using the previously constructed neural network-based hardness prediction system by the authors. Thus calculated hardness distribution in the cross sections of BMI penetration nozzle with different mounting angles (0°, 15°, 30°and 45°) was visualized as color chart maps in Fig. 12. In this study, the hardness was investigated by the Vickers hardness measured at a load of 9.8N for 20s.

Fig. 12(a) illustrates the hardness distribution in the cross sections (θ = 0° and θ = 180°) of BMI nozzle with the mounting angle of 0° after multi-pass welding (buttering and J-welding). Weld metal (WM) of Alloy 690 was shown in red color, and base metal (BM) of low-alloy steel A533B, SUS304 and Alloy 600 were shown in different grey colors, respectively. The hardness in HAZ of A533B steel was shown with rainbow colors depending on the different hardness levels. It can be seen that there are hardened ranges near the WM, but all the hardness in HAZ of BMI nozzle was lower than 350HV with the mounting angle of 0°. Similarly, when the mounting angle were changed from 15° to 45° as shown in Fig. 12(b)-(d), the hardness in the cross sections of BMI nozzle were lower than 350HV (the required specification in industry [6]). This illustrated the effectiveness of temper bead welding on decreasing hardness, and it proved that the chosen welding conditions of multi-pass welding were appropriate. And there was no remarked difference in the hardness distribution when the mounting angles changed from 0° to 45°, indicating that the mounting angle has insignificant effect on the hardness in the cross sections of BMI penetration nozzle.

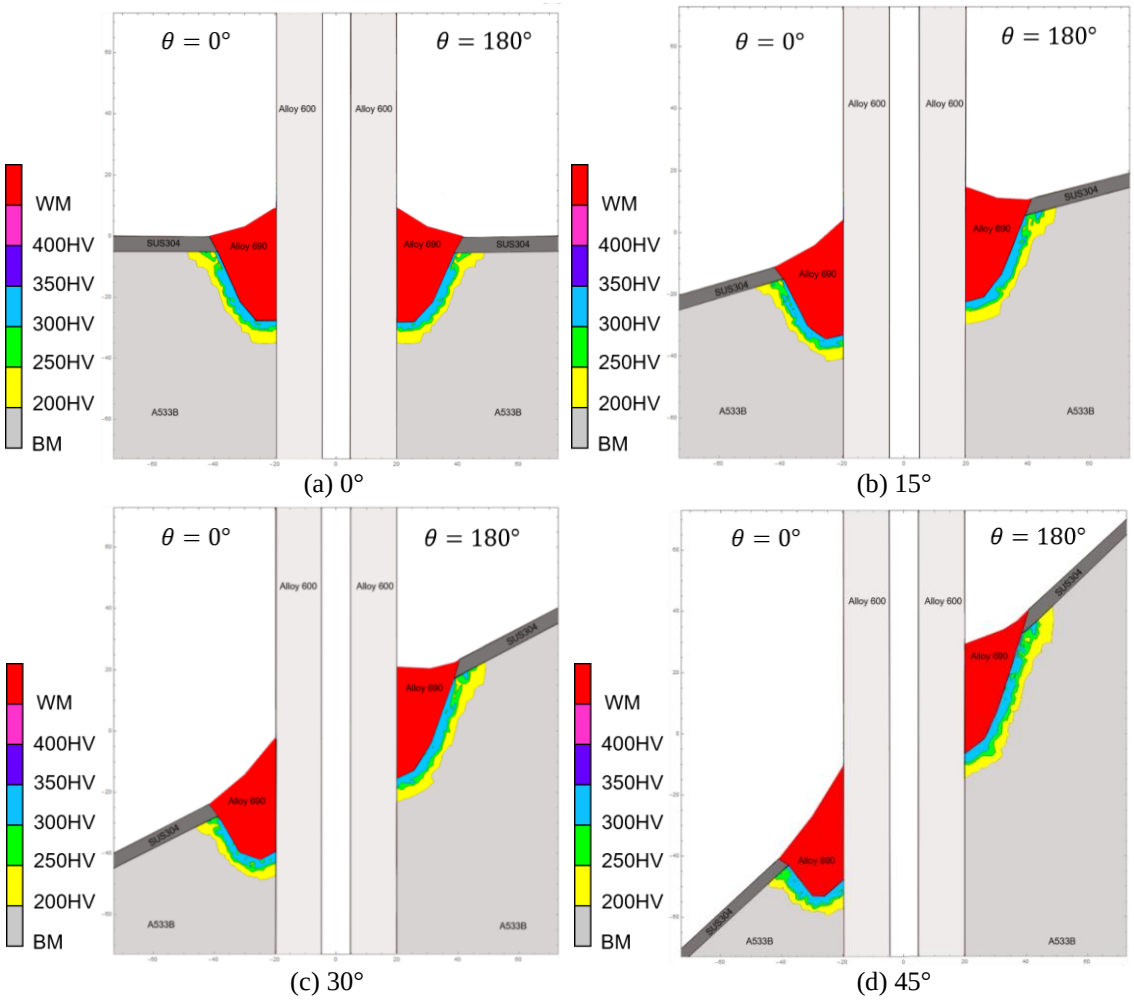

(a) 0° (b) 15°

(c) 30° (d) 45°

Fig. 12 Calculated hardness distribution in the cross sections of BMI nozzle with different mounting angles

6. Predicted toughness distribution in the cross section of BMI penetration nozzle with different mounting angles

Similarly, the toughness at every grid nodes of the cross section of BMI penetration nozzle was calculated based on the calculated thermal history at the grid nodes of the mesh, using the previously constructed neural network-based toughness prediction system. The calculated toughness distribution in the cross sections of BMI penetration nozzle with different mounting angles was visualized as color chart maps in Fig. 13. In this study, the toughness was investigated by the absorbed energy of Charpy impact test. Charpy impact test was carried out at 261K, which is the required test temperature of Charpy impact validity qualification test for temper bead welding in nuclear power industries. In order to avoid FPD (Fracture path deviation), side-notched Charpy V-notch specimens were prepared from samples subjected to the simulated thermal cycles. It should be noted that in the required specification in industry, there is absorbed energy 68J for standard Charpy impact test sample, which is equal to 40J for side-notched Charpy impact test sample used in the authors' study [7].

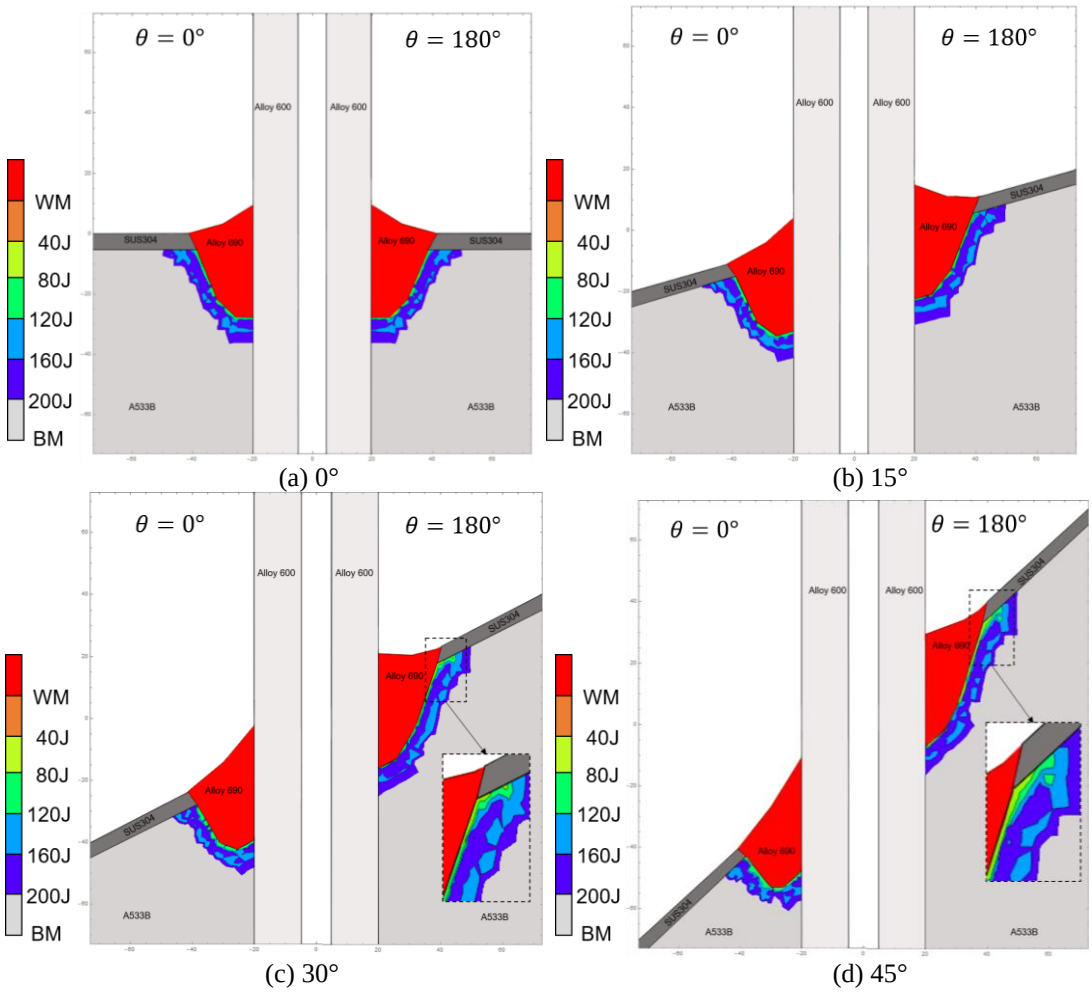

Fig. 13 Calculated toughness distribution in the cross sections of BMI nozzle with different mounting angles

When the mounting angle was 0°, the calculated toughness distribution in the cross sections (θ = 0° and θ = 180°) of BMI nozzle after multi-pass buttering and J-welding was illustrated in Fig. 13(a). WM of Alloy 690 was shown in red color, and BM of A533B steel, SUS304 and Alloy 600 were shown in different grey colors, respectively. The toughness in HAZ of A533B steel was shown with rainbow colors depending on the different toughness levels. It can be seen that there was low toughness zone near the WM, but all the toughness in HAZ of BMI nozzle was higher than 40J with

the mounting angle of 0°. Similarly, when the mounting angle were changed from 15° to 45° as shown in Fig. 13 (b)-(d), the toughness in the cross sections of BMI nozzle was found be higher than 40J (the required specification in industry), even when the mounting angle was changed to 45°. The calculated toughness results illustrated the effectiveness of temper bead welding on increasing toughness, and it proved that the chosen welding conditions of multi-pass welding were appropriate.

However, according to the toughness distribution with the mounting angle changed to 30° and 45° as shown in the magnified part of Fig. 13 (c)-(d), it was found that some low toughness zone (the absorbed energy between 40J and 80J) occurred in HAZ of the low-alloy steel A533B near to the SUS304 cladding layer in the section with θ of 180°, especially for the case of the 45° mounting angle. This indicated that the mounting angle has significant effect on the toughness in the cross sections of BMI penetration nozzle, which was different from hardness. Therefore, both hardness and toughness in the HAZ of repair welding need to be investigated to evaluate the tempering effect of temper bead welding for BMI penetration nozzle.

7. Benefits of the proposed method

It's well known that the BMI penetration nozzles have different geometric variables such as mounting angle, weld shape, nozzle thickness, nozzle outer radius, et al., according to the nozzle location and plant-specific design [1]. The geometric variables may affect the residual stresses as well as the mechanical property behaviors. In the previous study of Kim et al. [1], the geometric variables of BMI penetration nozzle such as mounting angle, nozzle thickness, seemed to have significant effect on the PWSCC initiation potential. However, in the study of Mochizuki et al. [2], the FEM residual stress analysis showed that the mounting angles and welding pass sequence conditions have small effect on the residual stress of J-welding of BMI penetration nozzles. Beside of the residual stresses, the mechanical properties are the key criteria to evaluate the temper effect of the repairing welding for BMI penetration nozzles. Therefore, the mechanical properties, such as hardness and toughness in the sections, which present the effects of various geometric variables, are very important to evaluate the temper effect of the repairing welding. In order to control the microstructure and the mechanical properties after welding, the appropriate welding conditions are necessary to be selected before the actual repair welding.

In this study, based on the FEM thermal history simulation of multi-pass circle welding, the hardness and toughness in the cross sections of BMI penetration nozzle with different mounting angles (0°, 15°, 30°and 45°) was successfully predicted using the proposed method. And the results showed that the mounting angle had insignificant effect on the hardness, however it had significate effect on the toughness in the cross sections of BMI penetration nozzle. Therefore, both hardness and toughness in the HAZ of repair welding need to be investigated to evaluate the tempering effect of temper bead welding for BMI penetration nozzle.

Using the proposed method, the hardness and toughness in the BMI penetration nozzle with different geometric variables such as mounting angle, nozzle thickness, et al., could be predicted prior to the actual multi-pass repair welding. It means that if the calculated hardness in HAZ is higher than the critical value, for instance more than 350HV (the required specification in industry), or the calculated toughness is lower than the critical value of 40J (the required specification in industry for side-notched Charpy sample), the welding conditions should be modified. Thus, the appropriate welding conditions can be selected prior to the actual repair welding for BMI penetration nozzle with different geometric variables. Therefore, the presently proposed method is greatly useful and effective for assessment of tempering effect of temper bead welding techniques for BMI penetration nozzle of the nuclear power plants.

8. Conclusions

A neural network-based prediction system for the hardness and toughness in BMI penetration nozzle with different mounting angles when temper bead welding technique was applied has been investigated. The following conclusions can be drawn:

(1) Based on the thermal history numerically obtained by FEM simulation, the hardness distribution and toughness distribution in the cross section of BMI penetration nozzles with different mounting angles (0°, 15°, 30°and 45°) was calculated, using the neural network-based hardness/toughness prediction system.

(2) The predicted hardness and toughness results showed that the mounting angle had insignificant effect on the hardness, however it had significate effect on the toughness in the cross sections of BMI penetration nozzle. Therefore, both hardness and toughness in the HAZ of repair welding needed to be investigated to evaluate the tempering effect of temper bead welding for BMI penetration nozzle.
(3) The proposed method was greatly useful and effective for assessment of tempering effect of temper bead welding techniques for BMI penetration nozzle of the nuclear power plants.

References

[1] J. S. Kim, M. S. Ra, K. S. Lee: "Investigation on the effects of geometric variables on the residual stresses and PWSCC growth in the RPV BMI penetration nozzles", Journal of Mechanical Science and Technology, Vol. 29, No. 3, pp. 1049~1064 (2015).
[2] M. Mochizuki, S. Okano, T. Kashiyama, Y. Niwa, M. Kameyama, M. Nakano: "Numerical Analysis of Residual Stress by J-weld and Repair Weld of Bottom Mounted Instrument Nozzles in Reactor Vessel Penetration", Proceedings of the 14th annual meeting of Japan Society of Maintenology, Japan, pp. 289-294 (2017).
[3] J. Liao, K. Ikeuchi, F. Matsuda: "Toughness Investigation on Simulated Weld HAZs of SQV-2A Pressure Vessel Steel", Nuclear Engineering and Design, Vol. 183, pp. 9-20 (1998).
[4] Y. Nakao, H. Oshige, S. Noi, Y. Nishi: "Distribution of Toughness in HAZ of Multi-Pass Welded High Strength Steel." Quarterly Journal of the Japan Welding Society, Vol. 3, pp. 773–781 (1985).
[5] N. Yurioka, Y. Horii: "Recent developments in repair welding technologies in Japan", Science and Technology of Welding & Joining, Vol. 11, pp. 255-264 (2006).
[6] L. Yu, Y. Nakabayashi, M. SaSa, S. Itoh, M. Kameyama, S. Hirano, N. Chigusa, K. Saida, M. Mochizuki, K. Nishimoto: "Neural network prediction of hardness in HAZ of temper bead welding using the proposed thermal cycle tempering parameter (TCTP)", ISIJ International, Vol. 51, pp. 1506-1515 (2011).
[7] L. Yu, M. SaSa, K. Ohnishi, M. Kameyama, S. Hirano, N. Chigusa, T. Sera, K. Saida, M. Mochizuki, K. Nishimoto: "Neural network-based toughness prediction in HAZ of low-alloy steel produced by temper bead welding repair technology", Science and Technology of Welding and Joining, Vol. 18, No. 2, pp. 120-134 (2013).
[8] D. Deng, H. Murakawa, M. Shibahara: "Investigations on welding distortion in an asymmetrical curved block by means of numerical simulation technology and experimental method", Computational Materials Science, Vol. 48, pp. 187-194 (2010).
[9] V. D. Manvatkar, A. Arora, A. De, T. DebRoy: "Neural network models of peak temperature, torque, traverse force, bending stress and maximum shear stress during friction stir welding", Science and Technology of Welding & Joining, Vol. 17, pp. 460-466 (2012).
[10] E. A. Metzbower, D. L. Olson, N. Yurioka: "Neural network analysis of oxygen in weld metals", Science and Technology of Welding & Joining, Vol. 14, pp. 566-569 (2009).
[11] D. Casasent, X. Chen: "Radial basis function neural networks for nonlinear Fisher discrimination and Neyman-Pearson classification", Neural Networks, Vol. 16, pp. 529-535 (2003).